Pharm Res (2014) 31:1855–1866
DOI 10.1007/s11095-013-1289-8

RESEARCH PAPER

# Specific Binding, Uptake, and Transport of ICAM-1-Targeted Nanocarriers Across Endothelial and Subendothelial Cell Components of the Blood–Brain Barrier

Janet Hsu • Jeff Rappaport • Silvia Muro

Received: 18 October 2013 / Accepted: 31 December 2013 / Published online: 21 February 2014


## ABSTRACT

***Purpose*** The blood–brain barrier (BBB) represents a target for therapeutic intervention and an obstacle for brain drug delivery. Targeting endocytic receptors on brain endothelial cells (ECs) helps transport drugs and carriers into and across this barrier. While most receptors tested are associated with clathrin-mediated pathways, clathrin-independent routes are rather unexplored. We have examined the potential for one of these pathways, cell adhesion molecule (CAM)-mediated endocytosis induced by targeting intercellular adhesion molecule -1 (ICAM-1), to transport drug carriers into and across BBB models.

***Methods*** Model polymer nanocarriers (NCs) coated with control IgG or antibodies against ICAM-1 (IgG NCs *vs.* anti-ICAM NCs; ~250-nm) were incubated with human brain ECs, astrocytes (ACs), or pericytes (PCs) grown as monocultures or bilayered (endothelial+subendothelial) co-cultures.

***Results*** ICAM-1 was present and overexpressed in disease-like conditions on ECs and, at a lesser extent, on ACs and PCs which are BBB subendothelial components. Specific targeting and CAM-mediated uptake of anti-ICAM NCs occurred in these cells, although this was greater for ECs. Anti-ICAM NCs were transported across endothelial monolayers and endothelial+subendothelial co-cultures modeling the BBB.

***Conclusions*** CAM-mediated transport induced by ICAM-1 targeting operates in endothelial and subendothelial cellular components of the BBB, which may provide an avenue to overcome this barrier.

J. Hsu • J. Rappaport • S. Muro
Fischell Department of Bioengineering
University of Maryland College Park
Maryland, USA

S. Muro (✉)
Institute for Biosciences and Biotechnology Research
University of Maryland College Park, 5115 Plant Sciences Building
College Park, Maryland 20742-4450, USA
e-mail: muro@umd.edu

**KEY WORDS** blood–brain barrier transport · brain endothelial and subendothelial cell layers · CAM-mediated endocytosis · clathrin- and caveolae-independent transport · ICAM-1-targeted nanocarriers

## ABBREVIATIONS

| | |
|---|---|
| ACs | Human astrocytes |
| ECs | Human brain microvascular endothelial cells |
| EIPA | 5-(N-ethyl-N-isopropyl)amiloride |
| FITC | Fluorescein isothiocyanate |
| ICAM-1 | Intercellular adhesion molecule-1 |
| IgG | Immunoglobulin G |
| MDC | Monodansylcadaverine |
| NC | Nanocarrier |
| PCs | Human brain vascular pericytes |

## INTRODUCTION

Our ability to treat medical conditions affecting the central nervous system (CNS) remains a formidable medical challenge because transport of most therapeutics across the blood–brain barrier (BBB) represents a major obstacle (1,2). The BBB controls the communication between the systemic environment and the brain, contributing to the regulation of the brain's homeostasis (3). At the cellular level, this structure is formed by endothelial cells (ECs) that constitute the inner surface of blood vessels in the brain microcirculation, as well as periendothelial cells that form a subendothelial lining, establishing direct contact with the endothelial component and the nervous tissue (2,4). Among these, pericytes (PCs) and astrocytes (ACs) represent the most abundant and studied cellular elements of the subendothelial side of the BBB (4). Both endothelial and subendothelial components contribute to the properties of this structure. For instance, ECs in brain capillaries and postcapillary venules possess distinct

characteristics from vascular ECs in most peripheral organs, such as the lack of fenestrations and special tightness of cell junction complexes (5). Subendothelial PCs and AC feet surround and communicate with the abluminal side of the endothelial lining and contribute to the regulation of the barrier function (4).

Transport across the BBB is rarely passive or between EC junctions that seal this cell monolayer (paracellular); instead, it occurs across cells (transcellular) (2). A number of strategies aim to bypass this structure by local administration into CNS compartments, enhancing the paracellular permeability, using the intranasal route, using exosomes, or via transcellular routing (6–9). With regard to the latter modality, transport of small molecules can be mediated by transporter proteins located at the EC membrane and larger molecules are mobilized via transcytosis, involving endocytic compartments that travel between the luminal and abluminal side of the endothelial lining (10,11). This process is often facilitated by binding of ligands to specific EC surface receptors, which is being explored for delivery of therapeutics (12). Some commonly targeted receptors in the BBB include insulin, transferrin, and low density lipoprotein receptors, which lead to transcytosis via the clathrin-dependent pathway (11). Although transport via such receptors has shown considerable success, brain entry of relatively bulky drug carriers (*vs.* smaller therapeutic conjugates) is often restricted due to size limitations of clathrin-coated compartments mediating transcytosis (12). Likewise, caveolae-mediated compartment formation poses even more restrictive size limitations than that of the clathrin route, and caveolae-mediated transcytosis has been reported to be down-regulated in the BBB (11,13). However, due to the potential of drug carriers to confer drug solubility, controlled circulation, protection from premature degradation, and timed release (14–16), it is compelling to explore new avenues to facilitate transcytosis of drug delivery systems across the BBB. An alternative is to target clathrin- and caveolae-independent mechanisms, yet there is very little knowledge on the occurrence of such routes in the BBB (8,17).

Within this latter category, an example which has rendered enhanced brain accumulation of drug carriers (i.e. bearing therapeutic enzymes) is that of targeting to intercellular adhesion molecule-1 (ICAM-1) (8,18–20). ICAM-1 is a cell surface molecule involved in inflammation and expressed on the vascular endothelium (including brain ECs) and other cell types, whose expression is up-regulated in most pathological states (21). Interestingly, targeting ICAM-1 with bulkier multivalent systems, such as model antibody-coated polymer nanocarriers (anti-ICAM NCs), induces endocytosis by a clathrin- and caveolae-independent mechanism called cell adhesion molecule (CAM)-mediated endocytosis (22). In contrast to other pathways, CAM endocytosis induces enzymatic-mediated remodeling of the plasmalemma composition (ceramide generation) at sites of carrier binding (23). This enhances the engulfment capacity of the membrane and allows efficient uptake of both nano- and micro-scale carriers, as demonstrated in cell cultures and mouse models (23,24). As an example of these differential properties of CAM- *vs.* clathrin-mediated endocytosis, targeting ICAM-1 with anti-ICAM NCs resulted in enhanced binding and uptake in EC cultures, as well as improved brain accumulation after intravenous (i.v.) injection in mice as compared to targeting the transferrin receptor (TfR) with anti-TfR NCs (20). This was despite the fact that: (a) anti-TfR antibodies in solution surpassed anti-ICAM antibodies with regard to these parameters and (b) both nanocarrier formulations displayed similar size, polydispersity, ζ-potential, and antibody coating density (20).

Importantly, we recently observed that targeting model polymer nanocarriers (~250-nm diameter) to ICAM-1 can also induce CAM-mediated transcytosis across cell monolayers without opening the cell junctions (25). This phenomenon was not observed when cells were cultured on solid impermeable substrates, but it occurred when they were grown on porous membranes that allowed formation of luminal and basolateral cell surfaces (25). However, this has been shown using model gastrointestinal epithelial cells (Caco-2) and whether a similar mechanism allows transcytosis across brain ECs is currently unknown. Also, whether cells of the subendothelial BBB lining, such as ACs and PCs, possess the ability to mobilize nanocarriers via the CAM-mediated pathway is an open question. In this study, we have explored this hypothesis using cellular mono- and co-culture models of the BBB, and found that this ICAM-1 targeting strategy may provide an avenue to overcome this barrier.

## MATERIALS AND METHODS

### Antibodies and Reagents

Monoclonal mouse anti-human ICAM-1 (anti-ICAM) was clone R6.5 (ATCC; Manassas, VA). Non-specific mouse IgG and secondary goat anti-mouse IgG were from Jackson Immunoresearch (West Grove, PA). FITC-like Fluoresbrite® polystyrene latex particles (not functionalized) were from Polysciences (Warrington, PA). $^{125}$Iodine ($^{125}$I) and Iodogen pre-coated tubes were purchased from PerkinElmer (Waltham, MA) and Thermo Fisher Scientific (Waltham, MA), respectively. Unless otherwise noted all other reagents were from Sigma Aldrich (St. Louis, MO).

### Preparation of ICAM-1-Targeted Nanocarriers

Model polymer nanocarriers were prepared by coating 100-nm diameter FITC-polystyrene particles by surface adsorption for 1 h at room temperature with unlabeled or $^{125}$I-labeled anti-ICAM (anti-ICAM NCs) or control IgG (IgG

NCs), as described previously (26). The concentration of particles and antibody in this coating mixture were ~$10^{13}$ particles/mL and ~700 μg of antibodies/mL. Non-coated antibody was removed by centrifugation at 13,800 g for 3 min and coated particles were re-suspended in phosphate buffered saline (PBS) supplemented with 1% bovine serum albumin to a concentration of ~$6.8\times10^{11}$ NCs/mL, followed by low power sonication to dissolve aggregates. Size, polydispersity index (PDI), and ζ-potential were measured by dynamic light scattering and electrophoretic mobility (Zetasizer Nano-ZS90, Malvern Instruments; Westborough, MA). The antibody coat density was assessed by measuring $^{125}$I content in a gamma counter (2470 Wizard2, Perkin Elmer; Waltham, MA).

## Cell Cultures

The three human cell types used in this study were NHA astrocytes (ACs; Lonza Walkersville, Inc., Walkersville, MD), brain microvascular endothelial cells (ECs; Applied Cell Biology Research Institute, Kirkland, WA), and brain vascular pericytes (PCs; ScienCell Research Laboratories, Carlsbad, CA). All cells were cultured in a 37°C, 5% CO2, and 95% humidity environment. For experiments on ICAM-1 expression and nanocarrier binding and uptake by cell monocultures, ECs were seeded at a density of $7.5\times10^4$ cells/cm$^2$ on gelatin-coated glass coverslips and grown in RPMI (Cellgro, Manassas, VA) supplemented with 20% fetal bovine serum (FBS), 2 mM glutamine, 30 μg/mL endothelial cell growth supplement, 100 μg/mL heparin, 100 U/mL penicillin, and 100 μg/mL streptomycin. ACs were seeded at a density of $5\times10^4$ cells/cm$^2$ on gelatin-coated glass coverslips and cultured in DMEM (Cellgro, Manassas, VA) supplemented with 15% FBS, 50 ug/mL gentamicin, 2 mM glutamine, 100 U/mL penicillin, and 100 μg/mL streptomycin. PCs were seeded at a density of $2.5\times10^4$ cells/cm$^2$ on poly-L-lysine-coated glass coverslips and cultured in Pericyte media (ScienCell Research Laboratories, Carlsbad, CA) supplemented with 20% FBS, 15 μg/mL pericyte growth factor, 100 U/mL penicillin, and 100 μg/mL streptomycin. For experiments mimicking transport across BBB models, ECs were grown to confluence on the apical side of 1.0-μm pore membranes (transwell inserts; BD Falcon, Franklin Lakes, NJ) in the absence (monocultures) or presence (co-cultures) of ACs or PCs on the basal side of the membrane, as previously described (27). Where indicated, cells were stimulated by incubation for 16 h with 10 ng/mL tumor necrosis factor α (TNFα) to induce pathological-like activation.

## ICAM-1 Expression on BBB Cells

Control or TNFα-activated cells were fixed with cold 2% paraformaldehyde, incubated with 8.3 μg/ml of anti-ICAM for 1 h at room temperature, and finally bound anti-ICAM was detected using 4.0 μg/ml FITC-labeled goat-anti-mouse IgG. Cell nuclei were stained with blue 4′,6-diamidino-2-phenylindole (DAPI). Samples were analyzed by fluorescence microscopy using Olympus IX81 microscope (Olympus, Inc., Center Valley, PA), ORCA-ER camera (Hamamatsu, Bridgewater, NJ), 40× objective (Olympus Uplan F LN; Olympus, Inc., Center Valley, PA) and DAPI, FITC, and Texas-Red filters (1160A-OMF, 3540B-OMF, 4040B-OMF; Semrock, Inc., Rochester, NY). Images were acquired with SlideBook 4.2 (Intelligent Imaging Innovations, Denver, CO) and analyzed using Image-Pro 6.3 (Media Cybernetics, Inc., Bethesda, MD) to estimate the mean fluorescence intensity.

## Binding and Internalization of Anti-ICAM NCs by BBB Cells

Control or TNFα-activated cells seeded on glass coverslips were incubated at 37°C with FITC-labeled anti-ICAM NCs (~$6.8\times10^{10}$ NCs/mL) for 1 h, 3 h, or 5 h. To evaluate the mechanism of uptake, experiments were conducted in the absence (control) or presence of pharmacological inhibitors of endocytic transport, including 3 mM amiloride (which inhibits CAM-mediated endocytosis), 1 μg/mL filipin (to block caveolae-mediated endocytosis), or 50 μM monodansylcadaverine (MDC; to inhibit clathrin-coated pits) (22). After the incubation time, carriers that did not bind firmly to cells were eliminated by removing the cell medium, cells were washed with PBS, and then fixed. Samples were then incubated with a Texas Red-labeled secondary antibody that recognizes and binds to anti-ICAM on the coat of carriers located at the cell surface, but cannot access anti-ICAM on the coat of carriers that have been internalized within cells (since cells were not permeabilized). This allows differential visualization of internalized *vs.* cell-surface bound carriers, which appear as green (FITC alone) *vs.* yellow (FITC and Texas Red), respectively. Samples were imaged by fluorescence microscopy using a 60× objective, FITC and Texas Red filters, and Image-Pro 6.3 was used as the image analysis software. The number of anti-ICAM NCs bound and internalized per cell were quantified as described (22). This was achieved using a macro that normalizes the area of specific fluorescence (over a threshold background) to the number of pixels that theoretically correspond to the size of a single particle, viewed under the magnification used to take the image. The percentage of internalization was then calculated as the fraction of internalized carriers as compared to the total number of carriers associated per cell, where the cell borders were identified by phase-contrast.

## Binding and Transport of Anti-ICAM NCs Across BBB Cell Models

Control or TNFα-activated cells were seeded at a density of $1.2\times10^5$ ECs/cm$^2$ and grown as confluent endothelial

monolayers alone or as endothelial (EC; above) + subendothelial (AC or PC; below) co-cultures using porous transwell membranes (27). $^{125}$I-anti-ICAM NCs or control $^{125}$I-IgG NCs were added to the apical chamber (~$6.8\times10^{10}$ NCs/mL) and incubated for 30 min. Non-bound carriers were removed as described above and samples were incubated at 37°C for additional time up to a total of 1 h or 5 h to allow potential transport (25). For mechanistic studies, incubation with $^{125}$I-anti-ICAM NCs was performed in the absence or presence of 33.3 μg/ml anti-ICAM to compete for binding, or 20 μM amiloride-derivative 5-(N-ethyl-N-isopropyl)amiloride (EIPA) to inhibit CAM-mediated transcytosis, as previously described (25). The amount of $^{125}$I-labeled carriers associated with each cell layer (endothelial or subendothelial), as well as the fraction transported to the basolateral chamber below the cells were recovered and quantified in a gamma counter. Free $^{125}$I was determined in each fraction using trichloroacetic acid (TCA) precipitation to subtract any potential contribution of free label to this measurement (25). Alternatively, FITC-labeled anti-ICAM NCs were incubated for 24 h at 37°C to allow visualization of carriers associated with the endothelial or subendothelial cell linings by fluorescence confocal microscopy (LM710 microscope; Zeiss, Oberkochen, Germany) using a 63× objective (Plan-APOCHROMAT; Zeiss, Oberkochen, Germany).

### Statistics

Data were calculated as mean ± standard error of the mean (SEM). Microscopy experiments contained duplicates, were repeated ≥2 independent times, and involved individual cell analysis (total ≥ 60 cells), where cells were randomly selected through the entire cell sample of ~$10^5$ cells. For radiotracing in transwells, experiments involved 4 replicates and were repeated ≥2 independent times. Statistical significance was determined as $p<0.05$ by Student's $t$-test.

## RESULTS

### Expression of ICAM-1 on Cells of the BBB

Using immunofluorescence, we first evaluated the level of expression of ICAM-1 on the surface of human brain cells which are known to form a part of the BBB, including microvascular endothelial cells (ECs), as well as astrocytes (ACs) and pericytes (PCs), cells that physiologically reside at the abluminal side of the endothelial lining of the BBB (4).

As shown in Fig. 1a, all three cell types expressed surface ICAM-1 under control conditions, although at relatively low levels (3-fold to 5-fold over background fluorescence), with both ACs and PCs displaying comparatively lower expression than ECs (88% and 76% of ECs, respectively). In all cases, incubation with TNFα to mimic a pathological stimulation

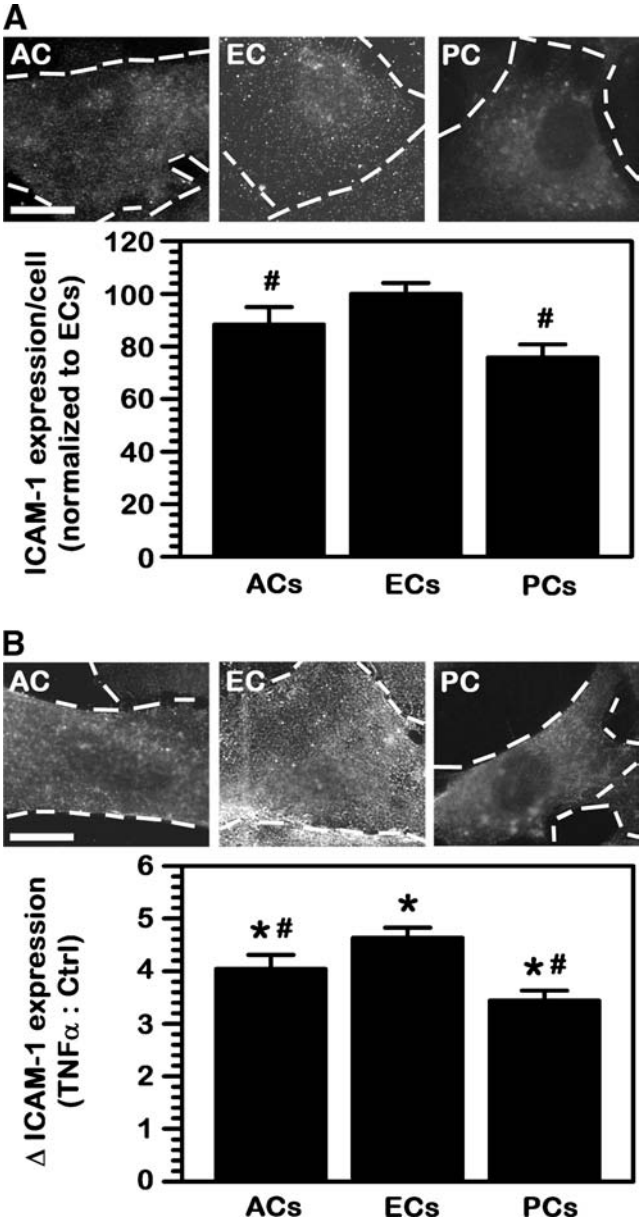


**Fig. 1** ICAM-1 expression on BBB cells. (**a**) Cell-surface ICAM-1 expression was tested using immunofluorescence on fixed human brain astrocytes (ACs), microvascular endothelial cells (ECs), or pericytes (PCs). Expression was quantified from microscopy images and normalized to the fluorescence level of ECs. (**b**) ICAM-1 expression on TNFα-stimulated cells (to mimic pathological activation) was assessed similarly and represented as fold enhancement (Δ) over control cells in (**a**). Scale bar = 10 $\mu$m. Data are mean ± SEM. #Comparison to ECs within each condition; *comparison between TNFα and control for each cell type ($p<0.05$ by Student's $t$-test).

enhanced ICAM-1 expression (Fig. 1b), as expected from the fact that ICAM-1 is upregulated in most disease states (21). For instance, using these culture models and detection system, ICAM-1 expression on the surface of ECs increased by 4.6-fold compared to control conditions. This level of enhancement was slightly lower for ACs (4.0-fold) and somewhat lower for PCs (3.4-fold). Therefore, both ACs and PCs still expressed

significantly lower absolute levels of ICAM-1 on their surface as compared to activated ECs (77% and 56% of ECs). This suggests potential for ICAM-1-targeting on the BBB, preferentially the EC lining and under disease conditions.

### Binding of Anti-ICAM NCs to Cells of the BBB

We then assessed the efficacy and selectivity associated with ICAM-1 targeting of drug carriers on these cells. As a model for a polymer nanocarrier we used FITC-labeled polystyrene nanoparticles coated with anti-ICAM (anti-ICAM NCs) or control IgG (IgG NCs). Since polystyrene is not biodegradable, this model allows tracking of targeting and transport (the focus of this study) without potential confounding effects of concomitant carrier degradation. The preparations had a size of 283±4 nm, PDI 0.18±0.01, ζ-potential −33±3 mV, and 222±8 antibodies/carrier for anti-ICAM NCs, and a size of 288±8-nm, PDI 0.18±0.02, ζ-potential −27±5 mV, and 170±8 antibodies/carrier for IgG NCs. These formulations have been characterized and found to be relatively stable (lack of aggregation, antibody detachment, and albumin coating (18,26)) and to render binding, endocytosis, intracellular trafficking, and *in vivo* circulation and biosdistribution comparable to biocompatible poly(lactic-co-glycolic acid) (PLGA) nanocarriers (28), which validates this model.

Pairing well with the observed presence of ICAM-1 on the surface of these BBB cells, fluorescence microscopy showed that FITC-labeled anti-ICAM NCs bound specifically to control ECs (51 NCs/cell vs 3 NCs/cell for non-specific IgG NCs) and also to both control ACs and PCs (40 NCs/cell and 57 NCs/cell, respectively; Fig. 2a). Also in agreement with ICAM-1 overexpression in pathologically conditions (21), binding of anti-ICAM NCs was enhanced in all three cell types upon TNFα stimulation, with the greatest increase observed for ECs (3.9-fold enhancement), followed by ACs (2-fold) and PCs (1.7-fold). Hence, the absolute binding was considerably greater for ECs (200 NCs/cell), followed by PCs (95 NCs/cell; 48% of ECs) and ACs (79 NCs/cell; 39% of ECs).

Furthermore, these differences were enhanced over time (Fig. 2b). For instance, binding of anti-ICAM NCs to ECs required the longest time in order to reach saturation ($t_{1/2}$ of 86 min), with a $B_{max}$ of 504 NCs/cell. ACs showed a $t_{1/2}$ of 70 min with a $B_{max}$ of 164 NCs/cell, and PCs saturated the fastest ($t_{1/2}$ of 8.2 min) with a $B_{max}$ of 104 NCs/cell. Therefore, at their respective saturation times, binding of anti-ICAM NCs to ECs surpassed binding to ACs and PCs by 3.1-fold and 4.8-fold.

### Endocytic Transport of Anti-ICAM NCs by Cells of the BBB

Since endocytic uptake represents a key step toward transport into the BBB or across this barrier (12), we next tested this

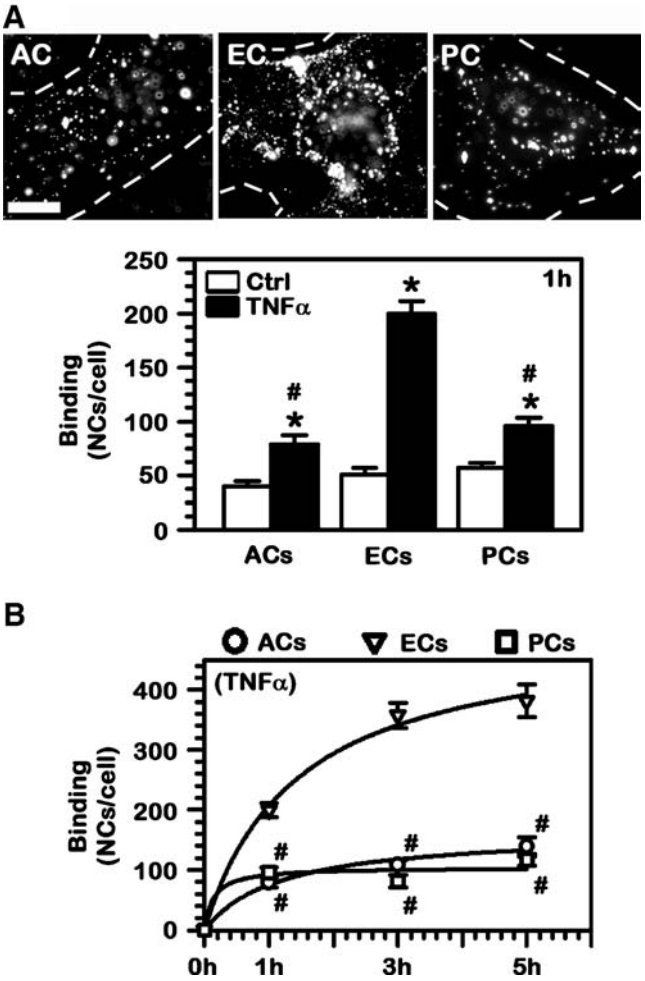


**Fig. 2** Binding of ICAM-1-targeted nanocarriers to BBB cells. (**a**) Binding of FITC-labeled anti-ICAM NCs to control or TNFα-activated human brain astrocytes (ACs), endothelial cells (ECs), or pericytes (PCs) was quantified by fluorescence microscopy after 1 h incubation at 37°C. Scale bar = 10 μm. (**b**) Binding of anti-ICAM NCs to TNFα-activated cells was assessed over a period of 5 h. (**a**–**b**) Data are mean ± SEM. #Comparison to ECs within each condition; *comparison between TNFα and control for each cell type ($p < 0.05$ by Student's *t*-test).

parameter. Using a well characterized method that allows differential fluorescent staining of cell-surface bound *vs.* internalized particles (see Methods), we observed that uptake of anti-ICAM NCs by all three cell types was relatively similar under control conditions (Fig. 3a). This rendered 18 NCs (ACs), 27 NCs (ECs), and 26 NCs (PCs) internalized per cell after 1 h. Yet, according to enhanced level of ICAM-1 expression and binding of anti-ICAM NCs observed under diseased conditions, TNFα resulted in an increased number of nanocarriers internalized by each of these cell types (Fig. 3a). Specifically, the number of anti-ICAM NC internalized into activated ECs significantly augmented by 4.1-fold over control conditions, while this increase was more moderate (yet still significant) in ACs (2.3-fold) and PCs (1.7-fold). These

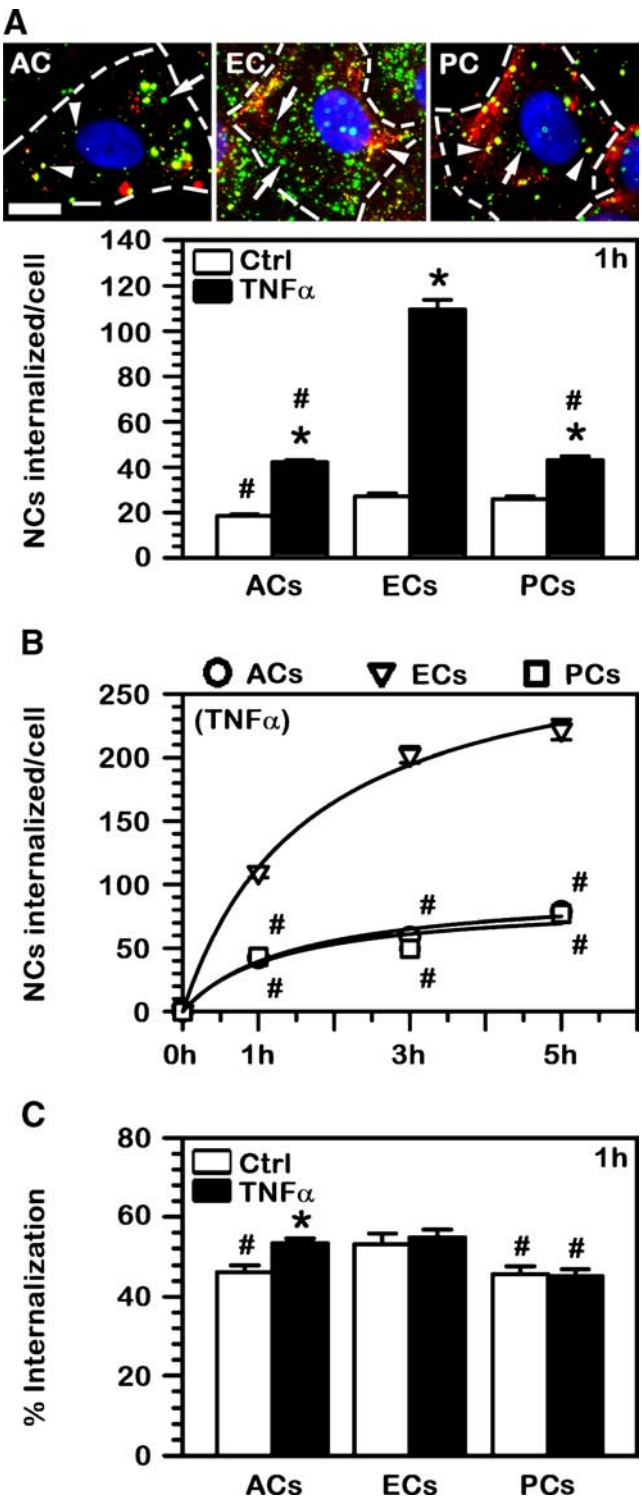


**Fig. 3** Internalization of anti-ICAM NCs into BBB cells. (**a**) FITC-labeled anti-ICAM NCs were incubated with TNFα-activated (images) or control human brain astrocytes (ACs), endothelial cells (ECs), or pericytes (PCs) for 1 h at 37°C. Non-bound carriers were washed, cells were fixed, and surface-located particles were immunostained with a Texas Red-secondary antibody (green FITC + Texas Red = yellow particles; arrowheads) versus internalized counterparts which remain single-labeled in green FITC (*arrows*). Scale bar = 10 μm. The absolute number of nanocarriers internalized per cell after 1 h incubation or (**b**) during a period of 5 h were quantified by fluorescence microscopy. (**c**) The percent of cell-associated particles that were internalized by cells was quantified as in (**a**). (**a**–**c**) #Comparison to ECs within each condition; *comparison between TNFα and control for each cell type ($p < 0.05$ by Student's *t*-test).

differences between ECs compared to ACs or PCs were further enhanced over time (Fig. 3b). For instance, the internalization $B_{max}$ was 302 NCs per EC, while this was 97 NCs per AC and 87 NCs per PC.

However, despite these differences, the efficiency of endocytosis (accounted as the number of nanocarriers internalized from the number of nanocarriers that initially bind to cells) was similar for all three cell types, ranging between 45% (PCs) and 55% (ECs) in control conditions (Fig. 3c). TNFα stimulation to mimic a diseased phenotype did not particularly affect the uptake efficiency and only ACs experience a slight enhancement from 46 to 53%. This suggests that the mechanism of endocytosis may be fairly similar for all BBB cells tested. Confirming this, amiloride, a pharmacological agent known to inhibit CAM-mediated endocytosis (22), significantly reduced uptake of anti-ICAM NCs by ACs, ECs, and PCs by 30–40% (Fig. 4). An inhibitor of caveolae-mediated endocytosis (filipin) did not have an effect on the uptake by either cell type. Interestingly, inhibition of clathrin-coated pits by monodansylcadaverine (MDC) differentially affected each cell type: it slightly reduced uptake by ACs (by 15%), it enhanced uptake within ECs (by 28%), and did not have an effect on PCs. Altogether, this indicates that, although uptake may be modulated or compensated by other pathways, CAM-mediated endocytosis is the main route for anti-ICAM NCs in BBB cells. Hence, this may render transport across said barrier similarly to the case of anti-ICAM NCs transport across epithelial linings (25).

## Binding and Transport of Anti-ICAM NCs Across Brain EC Monolayers

To assess if transport across ECs is possible, we grew confluent ECs monolayers on porous membrane transwell inserts and first looked at specificity of binding of $^{125}$I-labeled anti-ICAM NCs over control $^{125}$I-IgG NCs in this model (Fig. 5a). One hour after addition of anti-ICAM NCs to the apical chamber above control ECs, an average of $1.3 \times 10^6$ NCs were found to be associated per mm$^2$ area. This represents a 5-fold enhancement compared to non-specific IgG NCs and a similar specificity was maintained over a 5 h period. In addition, when ECs were activated with TNFα to mimic a pathological stimulation, anti-ICAM NCs surpassed control IgG NCs by 19-fold (1 h), validating the specificity of this interaction. Association of anti-ICAM NCs with TNFα-activated ECs decreased between 1 and 5 h (42% decrease), which could

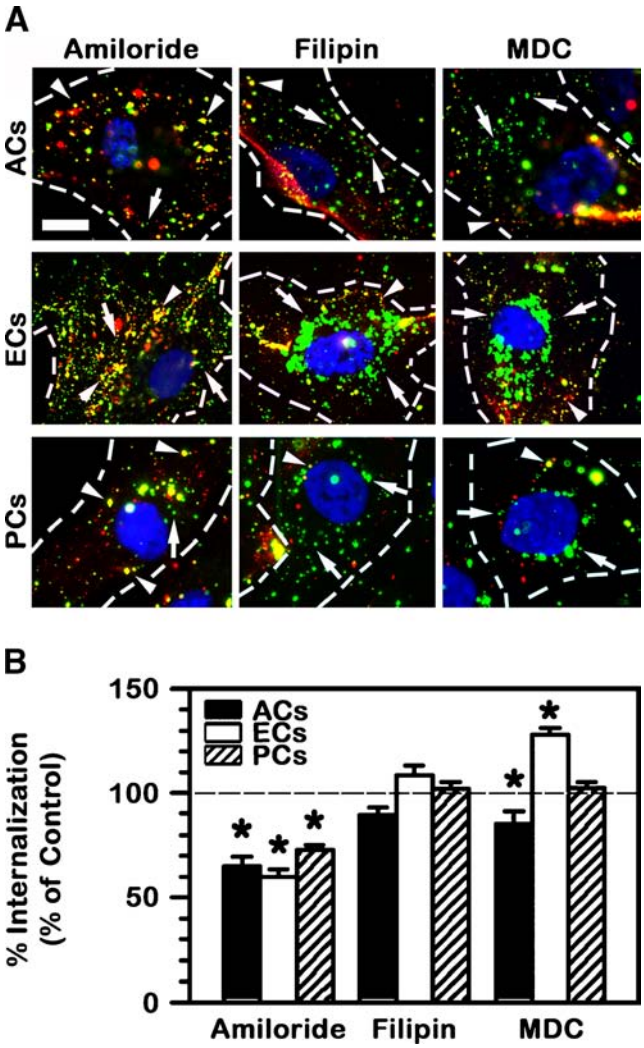


**Fig. 4** Mechanism of endocytosis of anti-ICAM NCs by BBB cells. (**a**) Uptake of anti-ICAM NCs by TNFα-activated human brain astrocytes (ACs), endothelial cells (ECs), or pericytes (PCs) was tested after 3 h incubation at 37°C in the presence of control cell medium or medium containing inhibitors of CAM-mediated endocytosis (amiloride), caveoli (filipin), or clathrin-coated pits (monodansylcadaverine, MDC). Surface-bound (*arrowheads*) *vs.* internalized nanocarriers (*arrows*) were visualized as described in Fig. 3 and compared to control conditions. Data are mean ± SEM. *Comparison to control (no inhibitor) condition for each cell type ($p < 0.05$ by Student's *t*-test). (**b**) The effect of endocytic inhibitors on the uptake of anti-ICAM NCs by TNFα-activated ECs is shown. Scale bar = 10 μm.

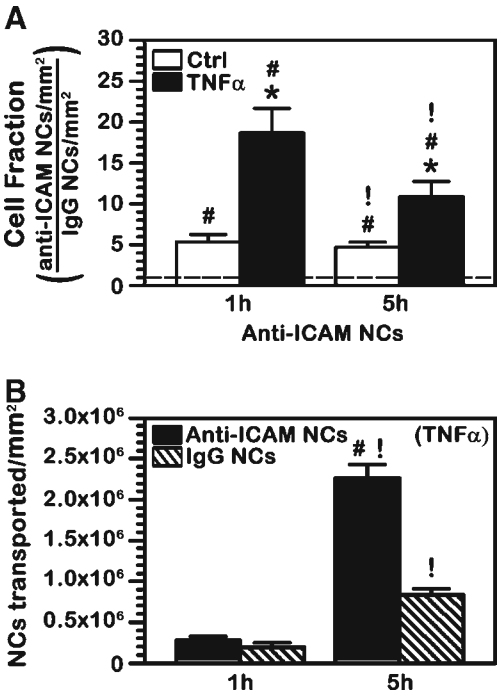


**Fig. 5** Binding and transport of anti-ICAM NCs across endothelial cell monolayers. (**a**) Control or TNFα-activated human brain microvascular endothelial cells were grown to confluence on porous membranes and $^{125}$I-anti-ICAM NCs were added to the apical chamber above the cells for 30 min to allow binding. Non-bound carriers were washed and cells were incubated at 37°C up to a total time of 1 h or 5 h. The radioisotope content of the cell samples was quantified to calculate the number of carriers associated per mm$^2$ surface. The graph shows the fold increase in binding of anti-ICAM NCs over that of control IgG NCs (dashed line = 1). (**b**) The absolute number of anti-ICAM NCs or IgG NCs transported to the basolateral chamber below the cells was also quantified. (**a**–**b**) Data are mean ± SEM. *Comparison between TNFα and control; $^{\#}$comparison between anti-ICAM NCs and IgG NCs; $^{!}$comparison between 1 h and 5 h for each condition ($p < 0.05$ by Student's *t*-test).

be due to transport of these carriers to the basolateral chamber below the cells.

When transport to the basolateral chamber was assessed over this period of time (Fig. 5b), no significant difference between anti-ICAM NCs and control IgG NCs was observed by 1 h. This level of detection may be the threshold of sensitivity of the method used or it may represent similar background non-specific leakage between cells. Importantly, the amount of anti-ICAM NCs detected in the basolateral chamber went up by 5 h (Fig. 5b). Although it appears that a fraction of non-specific leakage may contribute to said passage (the level of IgG NCs also increased in the basolateral chamber), specific transport is evidenced by the fact that the amount of anti-ICAM NCs below the cells surpassed by 3-fold that of IgG NCs at this time. Subtracting the value of non-specific penetration of IgG NCs from the level of transport observed for anti-ICAM NCs, it appears ~$1.4 \times 10^6$ anti-ICAM NCs were specifically transported per mm$^2$ of surface (Fig. 5b).

Also, in accord with the CAM-mediated pathway (22,25), presence of anti-ICAM in the cell media competed for binding of anti-ICAM NCs to EC monolayers (62% reduction; Fig. 6a) and consequently inhibited transport to the basolateral chamber (59% decrease; Fig. 6b). In addition, the presence of an amiloride derivative (EIPA) known to inhibit CAM-mediated transport (25) did not decrease binding of anti-ICAM NCs to EC monolayers (94% of control cells; Fig. 6a), as expected. However, EIPA affected transport to the basolateral chamber below the cells (54% reduction; Fig. 6b). This set of data demonstrates that binding to ICAM-

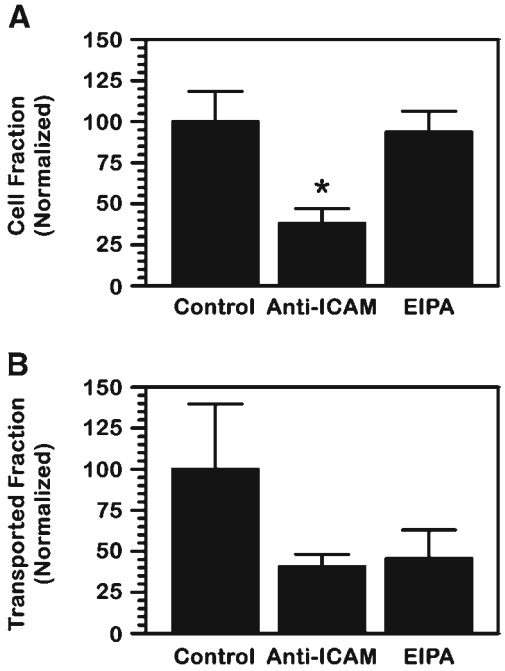


**Fig. 6** Mechanism of transport of anti-ICAM NCs across endothelial cell monolayers. Transport of $^{125}$I-anti-ICAM NCs across a monolayer of TNFα-activated human brain microvascular endothelial cells was assessed as in Fig. 5 in the presence of control cell medium or medium containing anti-ICAM (to compete for binding; 1 h transport) or an amiloride derivative (EIPA, to inhibit CAM-mediated transcytosis; 5 h transport). (**a**) The number of carriers associated per cell or (**b**) transported per cell to the basolateral chamber were quantified and normalized to control. (**a**–**b**) Data are mean ± SEM. *Comparison to control ($p < 0.05$, by Student's *t*-test).

1 is necessary for specific transport and this seems to be mediated by the CAM pathway.

## Transport of Anti-ICAM NCs Across BBB Endothelial and Subendothelial Cell Layers in Co-Cultures

To then evaluate transport of anti-ICAM NCs in a system that more closely mimics the endothelial (EC) lining and subendothelial (AC or PC) cell components of the BBB, we used co-culture models (EC-AC or EC-PC) (27). Endothelial monolayers were grown on the apical side onto porous transwell membranes, similar to the previous experiments. Either ACs or PCs (the subendothelial layer) were grown on the opposed basal side of the membrane which separated both cell types (27). All cells were treated with TNFα to mimic pathological stimulation. As represented in Fig. 7a, confocal microscopy showed the presence of FITC-labeled anti-ICAM NCs in association with the endothelial and subendothelial layers in each type of co-culture, after addition of said nanocarriers to the apical chamber above the cells.

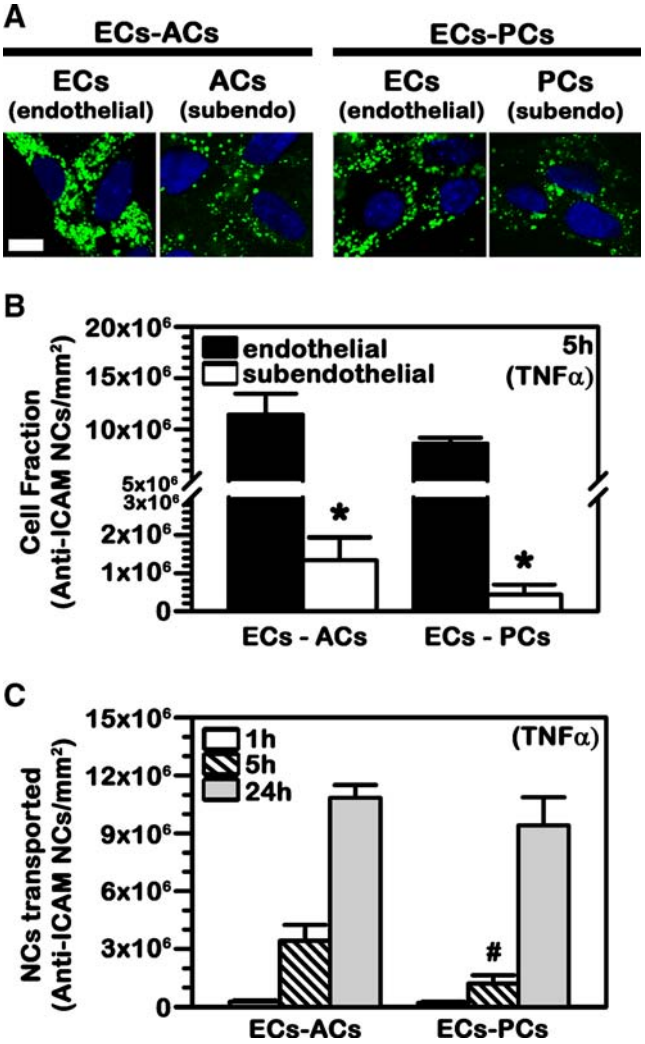


**Fig. 7** Binding and transport of anti-ICAM NCs across BBB cell bilayers. TNFα-activated human brain microvascular endothelial cells (ECs) were grown to confluence on the apical side of porous-membrane transwell inserts while activated astrocytes (ACs) or pericytes (PCs) were grown on the opposing basolateral side of the membrane (subendothelial layer). FITC-labeled or $^{125}$I-labeled anti-ICAM NCs were added to the apical chamber above the cells and incubations were carried at 37°C for 1 h, 5 h, or 24 h. (**a**) Confocal images of anti-ICAM NCs associated to the endothelial and subendothelial cell layers after 24 h incubation. Cell nuclei are stained with blue DAPI. Scale bar = 10 μm. (**b**) Total $^{125}$I-anti-ICAM NCs associated per mm$^2$ of endothelial *vs.* subendothelial layer after 5 h incubation. (**c**) Total $^{125}$I-anti-ICAM NCs transported per mm$^2$ of endothelial+subendothelial bilayers over time. (**b**–**c**) Data are mean ± SEM. *Comparison between the endothelial layer (ECs) and sub-endothelial layer (ACs or PCs); $^{\#}$comparison between the ECs-ACs bilayer and the ECs-PCs bilayer ($p < 0.05$ by Student's *t*-test).

To validate this finding and avoid potential visual interference of fluorescent carriers which may accumulate in the membrane between the cells, we used $^{125}$I-anti-ICAM NCs and separately quantified carriers associated with either the endothelial or subendothelial cell lining by scraping off each of these layers from the porous membrane. This confirmed

fluorescence microscopy results, revealing a greater association of anti-ICAM NCs with ECs *vs.* subendothelial ACs or PCs (8.5-fold and 20-fold difference respectively (Fig. 7b)). This pairs well with results on higher binding and uptake of anti-ICAM NCs by endothelial *vs.* subendothelial cells shown above (Fig. 2) and also validates the observation of transport of anti-ICAM NCs across EC linings (Fig. 5).

Importantly, transport of anti-ICAM NCs to the basolateral chamber below the cells was detected even in the presence of a subendothelial cell culture, both in the case of ACs and PCs (Fig. 7c): $2.6\times10^5$ to $2.1\times10^5$ NCs were transported per $mm^2$ after 1 h incubation, respectively. Said transport increased over time (e.g. 13.1-fold by 5 h and 41.5-fold by 24 h for EC-AC) and was slightly faster in the case of EC-AC *vs.* EC-PC co-cultures (2.8-fold difference over 5 h), although it reached similar levels for both models by 24 h.

## DISCUSSION

Efficient transport across the BBB is a key premise to achieve systemic drug delivery into the brain for treatment of CNS conditions (2,9). Targeting cell-surface receptors expressed on brain ECs, capable of transporting molecules transcellularly from the apical to the basolateral side of the endothelium (Fig. 8) has shown considerable promise to achieve this goal while preserving the permeability barrier in place between adjacent cells by avoiding the paracellular route (Fig. 8; (8,11)). While this has been amply explored by targeting clathrin-mediated pathways (caveoli seem restricted in brain ECs) (8,11), much less is known about clathrin- (and caveolae)-independent routes of transcytosis in the BBB (12,17). In this study we demonstrate that the route mediated by ICAM-1 (the CAM-mediated pathway) may be a promising alternative option since we found: (a) ICAM-1 presence and pathologically-induced overexpression on ECs and (at a lower extent) subendothelial AC and PC components of the BBB, (b) specific targeting and CAM-mediated uptake of model polymer anti-ICAM NCs by these cells, and (c) transport of said carriers across EC monocultures and endothelial-subendothelial co-cultures modeling the BBB.

ICAM-1 presence on the cell surface (*vs.* total expression) has been well established for brain ECs (29), but is less characterized for subendothelial brain cells in a manner comparative to the endothelium. In this regard, our data indicates that (apart from ECs) ICAM-1 was expressed on the cell surface of human brain ACs and PCs used in this study, and this surface-location was upregulated by pathological stimulation mimicked by TNFα. This is in accord with the literature indicating enhanced ICAM-1 expression by both ACs and PCs under the influence of inflammatory cytokines and during

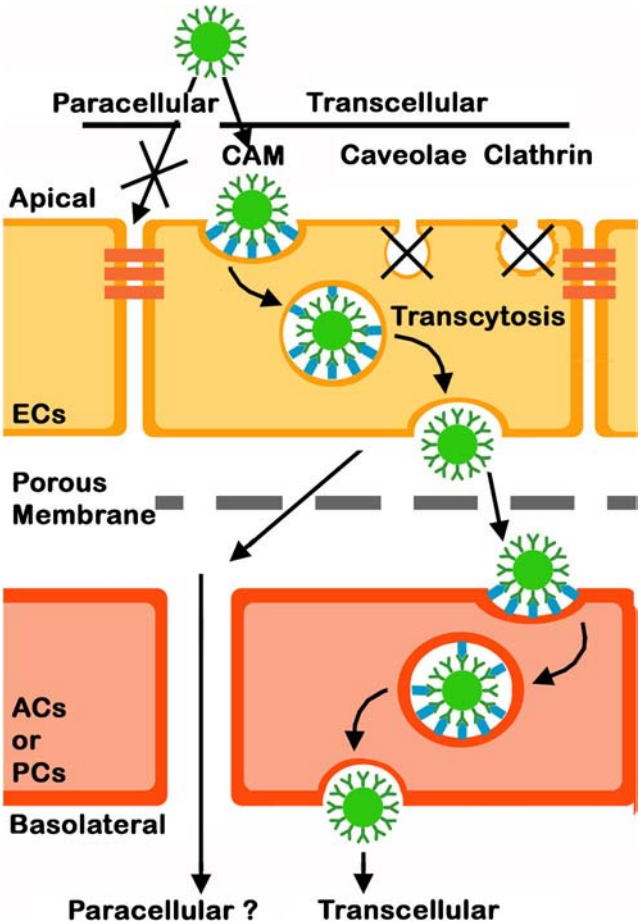


**Fig. 8** Schematic representation of the transport of anti-ICAM NCs across a co-culture model of the BBB. Anti-ICAM NCs bind specifically to ICAM-1 on the apical surface of endothelial cells (ECs) and induce endocytic uptake via the cell adhesion molecule- (CAM)-mediated pathway. This is a clathrin- and caveolae-independent mechanism, which results in transport of anti-ICAM NCs across the cell body via transcytosis (the transcellular route) *vs.* the paracellular route between adjacent cells. Anti-ICAM NCs are also endocytsed by astrocytes (ACs) and pericytes (PCs) underlining ECs and can traverse this subendothelial layer.

many brain pathologies (30–33). However, the level of expression under both control and disease conditions was lower for subendothelial cells as compared to endothelial counterparts, with PCs expressing the lowest amount of ICAM-1 amongst the three cell types tested. This indicates that BBB ICAM-1 may be more accessible to targeting from the endothelial side, as required when systemic administration is employed.

As per targeting by anti-ICAM NCs, specific and significant binding was also achieved in both endothelial and subendothelial cell cultures. Nanocarrier targeting was enhanced in disease-like conditions in all ACs, ECs, and PCs, and the absolute targeting level was again lower for subendothelial cells (particularly ACs) relative to ECs. In general, this result correlates with the pattern of ICAM-1 presence on these cells. However, some differences were

observed. As an example, for ECs the level of overexpression of ICAM-1 by TNFα was similar to the enhancement in anti-ICAM NC targeting (4.6-fold and 3.9-fold, respectively). However, for subendothelial cells the increase in nanocarrier targeting in disease over control cells was lower than the change in ICAM-1 expression observed for these conditions. Hence, it seems that not all surface ICAM-1 overexpressed during pathology is available for targeting on subendothelial cells. Nanocarrier binding is likely to depend on the receptor location, interaction with other molecular partners, etc. (apart from other factors), explaining this result (12,19). For instance, while PCs expressed the lowest ICAM-1 levels under control conditions, they afforded levels of anti-ICAM NC targeting greater than ACs and to the same extent as ECs. These examples illustrate that the relationship between target presence and its functional "targetability" is not always straightforward and this may also vary from one cell type to another. This is often underappreciated and makes success of targeting strategies somewhat unpredictable.

With regard to induction of endocytic transport by anti-ICAM NCs, the same internalized fraction was found for all cell types tested (~50% of the total number of cell-associated carriers by 1 h) and this parameter did not vary comparing control *vs.* disease conditions. This suggests that induction of the ICAM-1 pathway does not depend on the number of nanocarriers able to target the cell surface and rather endocytosis of each bound carrier is an independent event. This is in agreement with previous observations on this pathway obtained in other cell types (20), which may warrant transport without the need to surpass a certain targeting threshold. Because of this phenomenon, the absolute level of internalization of anti-ICAM NCs was entirely ruled by the absolute level of binding on cells. As a consequence, subendothelial cells internalized lower absolute levels of anti-ICAM NCs as compared to ECs, which was particularly evident under disease conditions (about half the EC level).

Altogether, the fact that ICAM-1 targeting and transport is viable for ACs and PCs is positive, since transport across the BBB will require that these features are not only present in ECs, but also in the subendothelial component of the BBB. Yet, lower ICAM-1 expression, anti-ICAM NC targeting, and absolute endocytosis by subendothelial cells *vs.* the endothelial counterpart may be beneficial to allow effective targeting from the endothelial apical side of the BBB (e.g., from the systemic circulation), high capacity for absolute transport by the endothelial lining (as observed), and low level of retention within the subendothelial layer in favor of further penetration into the brain parenchyma. Indeed, in a model where both the endothelial and subendothelial linings of the BBB were present (co-culture models), anti-ICAM NCs showed much higher association with ECs. Also, the presence of such subendothelial lining underneath the EC monolayer still allowed significant transport of carriers to the basolateral chamber, indicating that ICAM-1 targeting may represent an option for transport across the BBB. These data correlate well with enhanced brain accumulation of therapeutic agents (i.e. lysosomal enzymes) targeted via anti-ICAM NCs as compared to non-targeted counterparts (18–20,26).

With regard to the mechanism of transport (into and across cells; Fig. 8), this seems to be operated by the CAM pathway, as previously observed in the case of other cells types (22,25). Hence, ICAM-1 seems able to mediate transcytosis in cells that form barriers between separated compartments, including epithelial and endothelial linings ((25) and this work). This is in agreement with the biological function of this molecule. For instance, ICAM-1 serves as an adhesion molecule for leukocyte anchoring and extravasation in areas of inflammation, where multiple leukocyte-integrin copies bind multiple endothelial ICAM-1 molecules (21). Although paracellular extravasation of leukocytes between adjacent cells is mediated by several adhesion molecules (34), only ICAM-1 has been related to transcellular extravasation of leukocytes across EC body (35). Hence, ICAM-1 mediated transcytosis may be reminiscent of this function, which may explain the ability of this pathway to transport multivalent carriers better than monomolecular ligands (20), and to transport not only nanoscale but also micro-scale carriers (23,24). This may pose an advantage to drug delivery by avoiding size restrictions of other pathways, such as clathrin-related mechanisms (12). This helps explain enhanced brain accumulation of anti-ICAM NCs *vs.* anti-TfR NCs after i.v. injection in mice (20).

Interestingly, CAM-mediated transport of anti-ICAM NCs by BBB cells seemed influenced by the clathrin pathway, where inhibition of this pathway enhanced transport of anti-ICAM NCs by ECs while it decreased it in ACs. This is the first time that a dependence of the CAM route on another pathway has been observed (it has never been seen for ECs from other tissues) and it may be related to the function of the cellular components of the BBB. For instance, while ECs from most other origins display a diversity of pathways (clathrin-, caveolae-, phagocytosis-like, etc. (17,36)), endocytic transport in brain microvascular ECs seems restricted to the clathrin route (2,11), even though this lining is less permeable to solutes and needs to control blood-to-tissue communication more closely (3). Because of this, it is possible that common endocytic machinery (e.g., dynamin, cytoskeletal elements, motor proteins, SNARES, etc.) is "sequestered" by the clathrin pathway and not fully available for other endocytic routing. Inhibition of clathrin-mediated transport may "free" such common elements, allowing enhancement of the CAM pathway in brain ECs. In contrast, ACs regularly display additional endocytic routes (caveolae-mediated, phagocytic, etc. (37,38)) and such an effect would not be expected. Since ACs actively mobilize several toll-like and scavenger-like receptors associated to the clathrin route (37,38), it is possible that a small fraction of anti-ICAM NCs are not being specifically internalized by the CAM pathway but their antibody

component may interact with these other clathrin-associated receptors. Although ECs may also express these other receptors (36), it is possible that this route is avoided since activated ECs express higher levels of ICAM-1 compared to activated ACs. Indeed, anti-ICAM NCs bound at a much greater extent on activated ECs vs ACs.

Finally, aside from transport across the BBB for brain delivery, the findings in this study suggest that ICAM-1 targeting may also help transport therapeutic agents into the BBB itself. All three components of the BBB (EC, PC, and AC) can be subject to pathological dysfunction, which can be the cause and/or consequence of abnormalities that contribute to exacerbating brain pathology (30). For instance, PCs contribute to vasomodulation, endothelial proliferation and tissue repair, reinforcement of the permeability barrier, etc., and they have been involved in brain inflammation, viral infections, and many other CNS diseases (39). ACs are the most numerous cell type in the brain and are involved in brain development, supply of nutrients to neurons, modulation of synaptic communication, maintenance of the extracellular ion balance, scarring, etc., and have been associated with most CNS diseases as well (4,40). Hence, ICAM-1-mediated targeting and intracellular transport of therapeutics to these cells may help alleviate such maladies.

## CONCLUSION

ICAM-1 targeting induced endocytic transport of drug carriers into both endothelial (ECs) and subendothelial (ACs and PCs) components of the BBB in cell culture models. This could be exploited to deliver therapeutics to this lining in order to improve treatment of CNS conditions where these cells are involved (30). Binding and uptake capacity were highest for endothelial *vs.* subendothelial cells, which may provide a means to transport drug carriers across the endothelial lining while avoiding retention by immediate subendothelial cells. Indeed, ICAM-1 targeting provided nanocarrier transport across both endothelial and subendothelial layers, representing a new avenue for traversing the BBB. Transport was mainly operated via the CAM-mediated route, with only slight influence from the clathrin pathway. Therefore, non-classical endocytosis (such as ICAM-1-mediated CAM pathway) seems operative in endothelial and subedothelial cell components of the BBB and may offer alternative means to overcome this barrier for delivery of therapeutics into the brain. Future studies will focus on optimizing and testing this route in animal models.

## ACKNOWLEDGMENTS AND DISCLOSURES

This work was supported by NIH grant R01-HL09816 (S.M.).

## REFERENCES

1. Chen Y, Dalwadi G, Benson HA. Drug delivery across the blood–brain barrier. Curr Drug Deliv. 2004;1(4):361–76.
2. Pardridge WM. Biopharmaceutical drug targeting to the brain. J Drug Target. 2010;18(3):157–67.
3. Banks WA. Blood–brain barrier as a regulatory interface. Forum Nutr. 2009;63:102–10.
4. Abbott NJ, Ronnback L, Hansson E. Astrocyte-endothelial interactions at the blood–brain barrier. Nat Rev Neurosci. 2006;7(1):41–53.
5. Stevens T, Garcia JG, Shasby DM, Bhattacharya J, Malik AB. Mechanisms regulating endothelial cell barrier function. Am J Physiol Lung Cell Mol Physiol. 2000;279(3):L419–22.
6. Dhuria SV, Hanson LR, Frey 2nd WH. Intranasal delivery to the central nervous system: mechanisms and experimental considerations. J Pharm Sci. 2010;99(4):1654–73.
7. Lakhal S, Wood MJ. Exosome nanotechnology: an emerging paradigm shift in drug delivery: exploitation of exosome nanovesicles for systemic in vivo delivery of RNAi heralds new horizons for drug delivery across biological barriers. BioEssays. 2011;33(10):737–41.
8. Muro S. Strategies for delivery of therapeutics into the central nervous system for treatment of lysosomal storage disorders. Drug Deliv Transl Res. 2012;2(3):169–86.
9. Neuwelt E, Abbott NJ, Abrey L, Banks WA, Blakley B, Davis T, *et al.* Strategies to advance translational research into brain barriers. Lancet Neurol. 2008;7(1):84–96.
10. Minshall RD, Tiruppathi C, Vogel SM, Malik AB. Vesicle formation and trafficking in endothelial cells and regulation of endothelial barrier function. Histochem Cell Biol. 2002;117(2):105–12.
11. Pardridge WM. Blood–brain barrier delivery. Drug Discov Today. 2007;12(1–2):54–61.
12. Muro S. Challenges in design and characterization of ligand-targeted drug delivery systems. J Control Release. 2012;164(2):125–37.
13. Schnitzer JE. Caveolae: from basic trafficking mechanisms to targeting transcytosis for tissue-specific drug and gene delivery in vivo. Adv Drug Deliv Rev. 2001;49(3):265–80.
14. Duncan R. The dawning era of polymer therapeutics. Nat Rev Drug Discov. 2003;2(5):347–60.
15. Langer R. Drug delivery and targeting. Nature. 1998;392(6679 Suppl):5–10.
16. Torchilin VP. Multifunctional nanocarriers. Adv Drug Deliv Rev. 2006;58(14):1532–55.
17. Stan RV. Endocytosis pathways in endothelium: how many? Am J Physiol Lung Cell Mol Physiol. 2006;290(5):L806–8.
18. Hsu J, Northrup L, Bhowmick T, Muro S. Enhanced delivery of alpha-glucosidase for Pompe disease by ICAM-1-targeted nanocarriers: comparative performance of a strategy for three distinct lysosomal storage disorders. Nanomedicine. 2012;8(5):731–9.
19. Papademetriou IT, Garnacho C, Schuchman EH, Muro S. In vivo performance of polymer nanocarriers dually-targeted to epitopes of the same or different receptors. Biomaterials. 2013;34(13):3459–66.
20. Papademetriou J, Garnacho C, Serrano D, Bhowmick T, Schuchman EH, Muro S. Comparative binding, endocytosis, and biodistribution of antibodies and antibody-coated carriers for targeted delivery of lysosomal enzymes to ICAM-1 versus transferrin receptor. J Inherit Metab Dis. 2013;36(3):467–77.
21. Rothlein R, Dustin ML, Marlin SD, Springer TA. A human intercellular adhesion molecule (ICAM-1) distinct from LFA-1. J Immunol. 1986;137(4):1270–4.
22. Muro S, Wiewrodt R, Thomas A, Koniaris L, Albelda SM, Muzykantov VR, *et al.* A novel endocytic pathway induced by clustering endothelial ICAM-1 or PECAM-1. J Cell Sci. 2003;116(Pt 8):1599–609.
23. Serrano D, Bhowmick T, Chadha R, Garnacho C, Muro S. Intercellular adhesion molecule 1 engagement modulates

sphingomyelinase and ceramide, supporting uptake of drug carriers by the vascular endothelium. Arterioscler Thromb Vasc Biol. 2012;32(5):1178–85.
24. Muro S, Garnacho C, Champion JA, Leferovich J, Gajewski C, Schuchman EH, *et al.* Control of endothelial targeting and intracellular delivery of therapeutic enzymes by modulating the size and shape of ICAM-1-targeted carriers. Mol Ther. 2008;16(8):1450–8.
25. Ghaffarian R, Bhowmick T, Muro S. Transport of nanocarriers across gastrointestinal epithelial cells by a new transcellular route induced by targeting ICAM-1. J Control Release. 2012;163(1):25–33.
26. Hsu J, Serrano D, Bhowmick T, Kumar K, Shen Y, Kuo YC, *et al.* Enhanced endothelial delivery and biochemical effects of alpha-galactosidase by ICAM-1-targeted nanocarriers for Fabry disease. J Control Release. 2011;149(3):323–31.
27. Hatherell K, Couraud PO, Romero IA, Weksler B, Pilkington GJ. Development of a three-dimensional, all-human in vitro model of the blood–brain barrier using mono-, co-, and tri-cultivation Transwell models. J Neurosci Methods. 2011;199(2):223–9.
28. Muro S, Dziubla T, Qiu W, Leferovich J, Cui X, Berk E, *et al.* Endothelial targeting of high-affinity multivalent polymer nanocarriers directed to intercellular adhesion molecule 1. J Pharmacol Exp Ther. 2006;317(3):1161–9.
29. Wang X, Siren AL, Liu Y, Yue TL, Barone FC, Feuerstein GZ. Upregulation of intercellular adhesion molecule 1 (ICAM-1) on brain microvascular endothelial cells in rat ischemic cortex. Brain Res Mol Brain Res. 1994;26(1–2):61–8.
30. de Vries HE, Kuiper J, de Boer AG, Van Berkel TJ, Breimer DD. The blood–brain barrier in neuroinflammatory diseases. Pharmacol Rev. 1997;49(2):143–55.
31. Lee SJ, Drabik K, Van Wagoner NJ, Lee S, Choi C, Dong Y, *et al.* ICAM-1-induced expression of proinflammatory cytokines in astrocytes: involvement of extracellular signal-regulated kinase and p38 mitogen-activated protein kinase pathways. J Immunol. 2000;165(8):4658–66.
32. Proebstl D, Voisin MB, Woodfin A, Whiteford J, D'Acquisto F, Jones GE, *et al.* Pericytes support neutrophil subendothelial cell crawling and breaching of venular walls in vivo. J Exp Med. 2012;209(6):1219–34.
33. Yin L, Ohtaki H, Nakamachi T, Kudo Y, Makino R, Shioda S. Delayed expressed TNFR1 co-localize with ICAM-1 in astrocyte in mice brain after transient focal ischemia. Neurosci Lett. 2004;370(1):30–5.
34. Ley K, Kansas GS. Selectins in T-cell recruitment to non-lymphoid tissues and sites of inflammation. Nat Rev Immunol. 2004;4(5):325–35.
35. Millán J, Hewlett L, Glyn M, Toomre D, Clark P, Ridley AJ. Lymphocyte transcellular migration occurs through recruitment of endothelial ICAM-1 to caveola- and F-actin-rich domains. Nat Cell Biol. 2006;8(2):113–23.
36. Muro S, Koval M, Muzykantov V. Endothelial endocytic pathways: gates for vascular drug delivery. Curr Vasc Pharmacol. 2004;2(3):281–99.
37. Megias L, Guerri C, Fornas E, Azorin I, Bendala E, Sancho-Tello M, *et al.* Endocytosis and transcytosis in growing astrocytes in primary culture. Possible implications in neural development. Int J Dev Biol. 2000;44(2):209–21.
38. Sokolowski JD, Mandell JW. Phagocytic clearance in neurodegeneration. Am J Pathol. 2011;178(4):1416–28.
39. Armulik A, Genove G, Betsholtz C. Pericytes: developmental, physiological, and pathological perspectives, problems, and promises. Dev Cell. 2011;21(2):193–215.
40. Molofsky AV, Krencik R, Ullian EM, Tsai HH, Deneen B, Richardson WD, *et al.* Astrocytes and disease: a neurodevelopmental perspective. Genes Dev. 2012;26(9):891–907.